Journal of Computing and Information Technology - CIT 6, 1998, 2, 215–228

Volume Visualization of the Heart Using MRI 4D Cardiac Images

H. Abrishami Moghaddam and J. F. Lerallut

UTC/GBM UMR CNRS 6600, BP 20529, 60205 Compiègne, France

This paper deals with a system for volume visualization of the heart using multiphase-multislice cardiac MRI data. The proposed system is based on a generalized 4D form of a fuzzy object extraction algorithm in order to distinguish voxels belonging to cardiac object from noisy points and surrounding tissues. The system is initialized by interactive selection of a pixel placed inside the cardiac muscle in a slice. In some cases, complementary information might be necessary for segmentation because of the similarity in grey level information between the heart and surrounding tissues. We applied an active contour model and a contour propagation technique to a variance image for a rough segmentation of epicardium. The fuzzy approach in combination with the use of a deformable model for isolation enables us to segment cardiac object without modifying voxel grey levels and preserving anatomical details. Fuzzy object extraction involves problems of enormous combinatorial complexity, but this can be reduced by dynamic programming leading to practical algorithms for cardiac data sets. We have implemented these algorithms and tested their efficiency in preserving heart data during preprocessing. Different anatomical presentations of the heart have been used for this purpose, consisting of only a small number of slices per volume.

Keywords: Volume Visualization, Cardiac MRI, Fuzzy Object Extraction, Deformable Models.

1. Introduction

Anatomical 3D visualization of human organs using large 3D medical data sets which result from routine Magnetic Resonance Imaging examinations has been the subject of a large amount of research work during the last two decades. Most of this work was made on static organs (e.g. head) where a relatively good spatial resolution is available in a short acquisition time. With the introduction of cardiac MRI and the availability of 4D volumetric time-varying data sets, a new perspective in cardiac image analysis and visualization appeared, promising a more accurate non-invasive quantification of local, regional and global function of cardiac cavities and 3D dynamic anatomical visualization of the heart with a minimal interaction of specialist. Clinical cardiac MRI studies consist of a large number of images, about 80-100, from which qualitative information about heart function and its anatomy can be obtained by viewing the images in a sequence.

Several automatic or semi-automatic, 2D or 3D based methods of varying complexity and precision have previously been proposed to detect cardiac boundaries and to dynamically visualize cardiac cavities using surface reconstruction techniques. Ranganath [Ranganath 1995] presented a contour extraction method based on snakes proposed by Kass *et al.* [Kass et al. 1987]. In this work a contour propagation technique was introduced in order to automatically propagate cardiac contours along the slices in a volume and through different phases. A 3D surface reconstruction of left ventricular cavity at systole and diastole using this method was presented by Abrishami *et al.* [Abrishami et al. 1996]. Such models [Cohen and Cohen 1990, Ranganath 1995, Chakraborty et al. 1996] were generalized in $2\frac{1}{2}$D and 3D [Terzopoulos et al. 1988], where the deformable surface evolves under the forces computed on a 2D image or a set of 2D images. In contrast to these approaches, Cohen *et al.* [Cohen et al. 1992] and McInerney and Terzopoulos [McInerney and Terzopoulos 1993] developed a 3D deformable shape model, based on a variational approach and a finite element method to express the surface in a discrete basis of continuous functions.

Application of the method to MRI data of human heart and CT data of canine heart in order to reconstruct the left ventricle (LV) shape have been reported by these authors, respectively. A new family of parametric models, deformable superquadrics [Terzopoulos and Metaxas 1991], were successfully applied to 4D cardiac images for shape description and particularly for quantitatively analyzing the deformation of the LV [Bardinet et al. 1994]. Shi *et al.* [Shi et al. 1994] developed another approach using the shape properties of the endocardial-epicardial LV surfaces in order to compute point-wise myocardial motion vector fields between successive image frames through the entire cardiac cycle. A recent non-invasive technique, the magnetic resonance (MR) tagging of myocardium [Axel and Dougherty 1989, Zerhouni 1988], has been used as an alternative quantitative approach, which creates a magnetization grid that tags the underlying tissue, and uses the grid deformation to follow the tissue movement over a gated sequence [Amini et al. 1994, Park et al. 1996a]. Amini *et al.* proposed an energy minimizing B-*spline* snakes for tracking myocardial tag lines in 2D slices and computed myocardial quantitative parameters like strain (Amini *et al.* 1994). Park *et al.* developed a new class of deformable 3D *surface* (Park *et al.* 1996*a*) and em volumetric [Park et al. 1996b] models and applied them to a tagged MRI data set to extract contraction, twisting and rotation motion of the LV myocardium. Inspired by (Park *et al.* 1996*b*), Declerk *et al.* [Declerck et al. 1996] defined a 4D polar transformation and proposed a method to track the motion of the LV, approximating the shape of the LV as a stretched sphere in the long axis direction of the heart.

In most of these works, a relatively simplified surface model of the heart (almost the LV) has been used. In spite of the clinical value of the LV surface reconstructions and extracted parameters of the LV function, dynamic 3D volume visualization of the heart with anatomical details of cardiac structures has a number of attractive properties which make it useful for diagnostic and surgical planning purposes [Vannier et al. 1989]. Here, there is no need for simplifying geometrical constraints; indeed, pre processing algorithms try to preserve maximum information in the image as well as voxel grey levels which contain valuable information for the specialist. With the progress in cardiac MRI, and the availability of real time high resolution volumic images [Irarrazabal et al. 1995, Pauly et al. 1996], such anatomical views of the patient's heart can be used as a platform for the analysis, education and surgery simulation purposes. Several researchers have developed methods and platforms for volume visualization of medical data [Höhne 1995, Avila et al. 1994, Udupa et al. 1993] and electronic atlases of rigid or static human organs have been created [Höhne et al. 1992]. However, a limited amount of previous works was made on volume visualization of the heart [McVeigh et al. 1994]. The major difficulties with cardiac MRI are: *i*) low spatial and temporal resolutions, *ii*) poor quality of the image due to noisy points and non-distinctive intensity pattern of the heart compared with surrounding tissues and *iii*) long acquisition time. In this paper, we pre sent a new method for automatic segmentation of the heart based on a generalized 4D fuzzy object extraction algorithm. The idea is to take into consideration the inherent data inaccuracies and the fuzziness of voxel intensity information. A fuzzy object is defined by a set of voxels which are connected to an initial point selected inside the object of interest. All the grid points in the image are examined and a measure of connectedness (a number between 0 and 1) is attributed to them. Because of the similarity in grey level information between the heart and surrounding tissues, complementary information might be necessary to isolate the cardiac object. For this purpose, we have included motion information of the heart in the form of a variance image and obtained a rough segmentation of the epicardium using deformable models.

The paper is organized as follows: Cardiac MRI data and image characteristics are described in the next section. The fuzzy object extraction is presented in section 3. Section 4 presents a brief review of snakes and its application for a rough segmentation of the epicardium. The results and discussions are given in section 5 and section 6 presents the conclusions.

2. Cardiac MRI Data

2.1. Data Acquisition

The data set provided by cardiac MRI is essentially 4D, consisting of 8-12 cross-sectional tomographic slices imaged at 8-16 cardiac phases. The image resolution and signal-to-noise ratio (S/N) of each voxel are determined by the field-of-view (FOV), slice thickness and the size of the acquisition matrix. In addition, the S/N is determined by the number of acquisitions and therefore by the duration of measurement. FOV values of 300-400mm (also 250mm for children due to smaller anatomy) is a good compromise between S/N, image resolution and measurement time. S/N is also proportional to slice thickness and therefore the slice should not be too thin when selected. For cardiac imaging of adults, 8-10mm generally provides good anatomical resolution. It should be noted, however, that in some cases (very slow blood flow) with spin echo techniques, thinner slices of 5-6mm may be necessary to achieve sufficient signal loss of flowing blood. The slice thickness for children or babies should be selected at around 5-7mm [Siemens 1992]. In the following, we will review four different sequences which can be used in cardiac examinations:

- **Spin echo:** The ECG triggered spin echo (SE) sequence is specially useful with cardiovascular examinations of the soft tissue anatomy and a relatively clear contrast appears both between the different types of soft tissue and between the soft tissue and flowing blood. With SE technique, only a single line of data can be acquired per cardiac function (TR). A complete image typically requires 128-512 lines and thus 128-512 repetitions of the pulse sequence. This limitation essential ly precludes a conventional SE sequence from being used for fast imaging.

- **Gradient echo:** In MRI of the cardiovascular system, gradient echo (GE) sequences are specially advantageous for the dynamic visualization of blood flow and Cine-MR imaging. In general, the contrast of soft tissue is not as good as with the SE sequences. The advantage of GE sequences is the possibility to use short repetition times in order of 50ms which allows 3D acquisitions in a reasonable time period (e.g. 5-10 minutes). 3D has the advantage of allowing very thin (e.g. 1mm or less), contiguou s sections with good contrast and S/N.

- **TurboFLASH:** With the addition of a radio frequency preparatory pulse, scan times of less than 1 second are feasible with GE sequences. This approach called turboFLASH (Fast Low Angle SHot) can be used in conjunction with contrast administration to obtain perfusion images of the heart in less than 1 minute [Edelman 1995].

- **Echo Planar:** Echo planar imaging (EPI) requires substantial hardware modifications and therefore, is not yet in widespread use. Using modified hardware, a complete image can be acquired in as little as 30ms. There are SE and GE variants of EPI which may prove particularly useful for anatomic, functional, and perfusion imaging of the heart.

2.2. Data Description

Cardiac MRI studies provide a representation of four main constituents of the chest cardiac region, i.e., muscle, fat, blood and air (lungs). Their appearance in images depends on the pulse sequence used. In SE images, regions of blood flow appear dark, whereas in GE images, they appear bright (Fig. 1). In both types of studies, muscle has mid-grey intensities and air is dark. Fat appears bright relative to muscle in both types of studies, though this contrast seems larger in SE. Fig. 1(a) and (b) show two different localization views used to obtain short axis images. A transverse view at the ventricular level (Fig. 1(a)) and a long axis view (Fig. 1(b)) have been used as first and second localizers. MR images in the short axis view provide good evaluation of the lateral wall, septum and the papillary muscles of the left ventricle. Fig. 1(c), (d) and (e) show GE images taken at the base, middle and apical levels, respectively. Some anatomical points have been highlighted in the images. At the base, the ventricular outflow tracts appear, changing the anatomy substantially compared to the lower levels (Fig. 1(c)). Fig. 1(d) shows the presence of the papillary muscles within the blood pool. These appear darker than blood in GE images and lighter in SE. Dark regions within the blood pool in Fig. 1(d) taken just below the base are due to signal loss from turbulent blood flow. Fig. 2(a) shows a typical SE axial image of the heart in ventricular plane. A granular noise due to the pulsatile

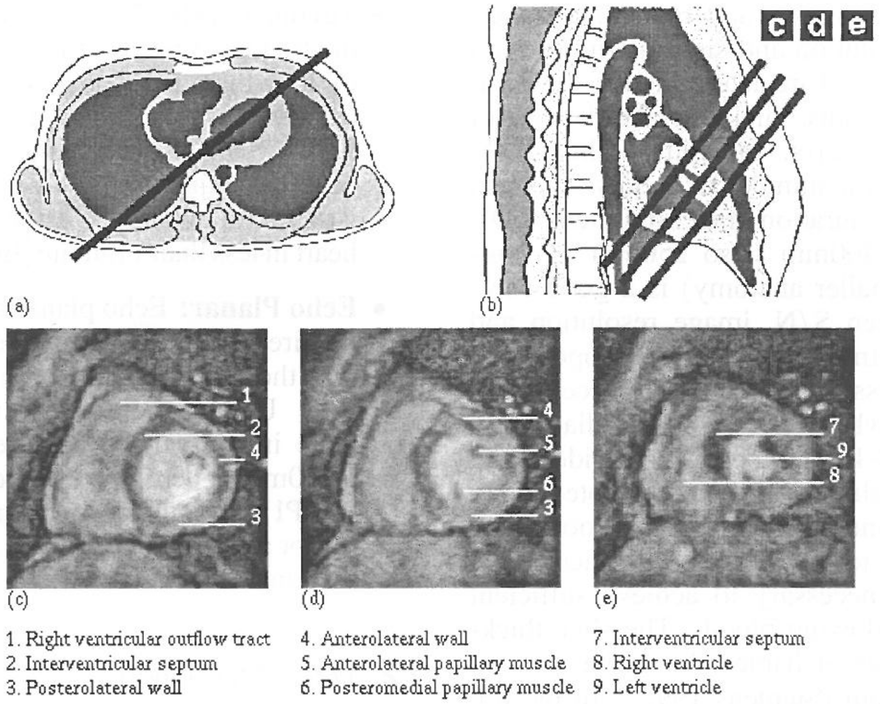

Fig. 1. MR gradient echo images in the short axis view (a) first localizer: Transverse (axial) view at the ventricular level, (b) second localizer: long axis view, (c),(d) and (e) heart in three different slices at base, middle and apex levels. Some anatomical points have been highlighted in the images.

blood movement, superposed on the image, is visible. These artifacts are particularly present on transversal slices at the aorta level which complicates the image interpretation [Desgrez et al. 1994]. A series of 4D SE slices has been shown in Fig. 2(b). The image is composed of 5 different slices (rows) through 5 different time phases (columns). In our data sets (both SE and GE), we have found the image quality to be worse when the heart expands from systole to diastole, exhibiting contrast loss, noise, and spurious detail. This is due to the rapid expansion of the heart and motion out of plane at this stage of the cycle. The best images are usually found at diastole, when the ventricles are filled with blood and the heart is relatively stationary.

3. Fuzzy Object Extraction

As mentioned above, different sources like pulsatile or low speed blood movement, degrade cardiac MRI images. These artifacts and moreover, data inaccuracies due to the echoes of structures near or attached to myocard like papillary muscles, involve uncertainty about identification of the pixels representing the cardiac object. Since the heart has not an intensity pattern distinctly different from other objects and due to the fuzziness of image information, application of ordinary segmentation techniques in a hard sense to segment the cardiac object is not satisfactory. In order to consider these inherent inaccuracies, we applied a recently formulated fuzzy object extraction algorithm [Udupa and Samarasekera 1996]. In the following, we will briefly review this method and demonstrate its use for segmentation of the heart. For a detailed discussion on this technique we refer the reader to Udupa and Samarasekera [Udupa and Samarasekera 1996].

3.1. Fuzzy Object Definition

Objects in images have two important characteristics. First, they have a graded composition. In the SE slice of the heart shown in Fig. 2(a), for example, the object called 'LV cavity' consists of both the blood (dark region) as well as of the brighter noisy regions due to blood movement. Second, the image elements that constitute an object hang together in a certain way. Again consider Fig. 2(a) which consists

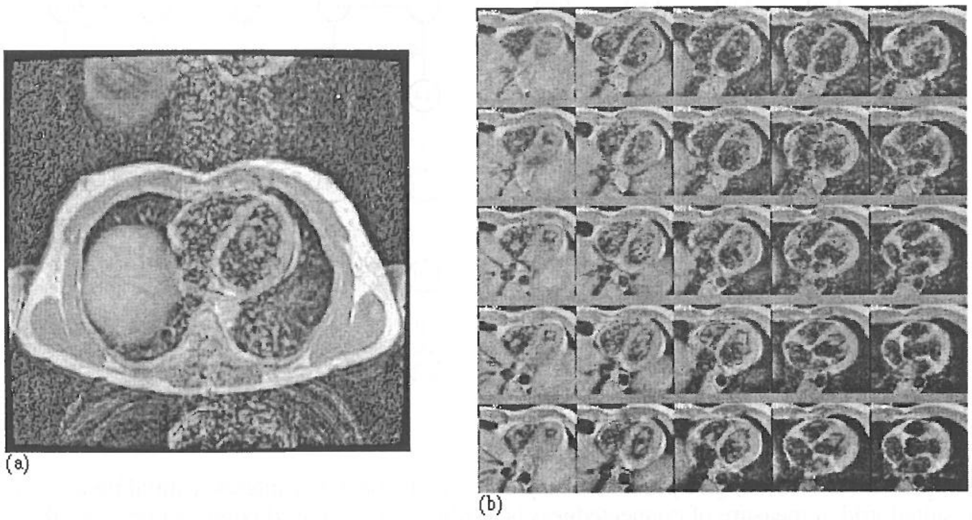

Fig. 2. (a) A middle slice spin echo image of the heart (axial view) before selecting the area of interest. The noise due to pulsatile blood movement can be observed. (b) a series of 4D spin echo axial slices. Images in each column represent a slice of the heart imaged at five different time phases.

of two ventricular cavities. The pixels that constitute the LV, including those repres enting the blood and noisy pixels, hang together to form an object called ventricular cavity much more strongly than the pixels that represent blood in the two ventricles, although they have very similar intensity properties (because of the presence of interventricular septum). Both these graded composition and hanging togetherness are fuzzy properties and can be used to define a notion of fuzzy object. Moreover, independent of any image data, there is a fuzzy adjacency relation (the closer the points are, the more adjacent they are to each other) between image elements. In the following we remind of the two known definitions of fuzzy subset theory: *fuzzy subset* and *fuzzy relation* [Zadeh 1965, Kaufmann 1975]. Let X be any reference set. A *fuzzy subset* $\mathcal{A}$ of X is a set of ordered pairs

$$\mathcal{A} = \{(x, \mu_{\mathcal{A}}(x)) | x \in X\}, \tag{1}$$

where

$$\mu_{\mathcal{A}} : X \longrightarrow [0, 1] \tag{2}$$

is the *membership function* of $\mathcal{A}$ in X. A *fuzzy relation* ρ in X is a fuzzy subset of X × X

$$\rho = \{((x, y), \mu_\rho(x, y)) | (x, y) \in X \times X\}, \tag{3}$$

where

$$\mu_\rho : X \times X \longrightarrow [0, 1] \tag{4}$$

The aim of fuzzy object definition is to capture the global phenomenon of hanging togetherness in a fuzzy relation between grid points, called "connectedness". We do this first through a local fuzzy relation, κ, called "affinity". Affinity takes into account the degree of adjacency of the grid points as well as the similarity of their intensity values. The closer the grid points are and the more similar their intensities are, the greater is the affinity between them. The membership function of the affinity between two grid points c and d in an image, $\mu_\kappa(c, d)$, is defined by:

$$\mu_\kappa(c, d) = \mu_\alpha(c, d) h(f(c), f(d)), \tag{5}$$

where $\mu_\alpha(c, d)$ represents the membership function of the fuzzy adjacency relation between c and d which can be defined as follows:

$$\mu_\alpha(c, d) = \begin{cases} 1, & \sqrt{\sum_i (c_i - d_i)^2} \leq 1 \\ 0, & \mathit{otherwise.} \end{cases} \tag{6}$$

and $h(f(c), f(d))$ can be selected as follows:

$$h(f(c), f(d)) = e^{-(1/2)[((1/2)(f(c)+f(d))-m)/s]^2} \tag{7}$$

In this equation $f(c)$ and $f(d)$ are simply the intensity of grid points and m and s are the mean intensity and the standard deviation of grid points which belong to the object of interest. To see how affinity is used to assign a "strength of connectedness" to any pair of grid points, consider all possible connecting "paths" of grid points between o and c (Fig.

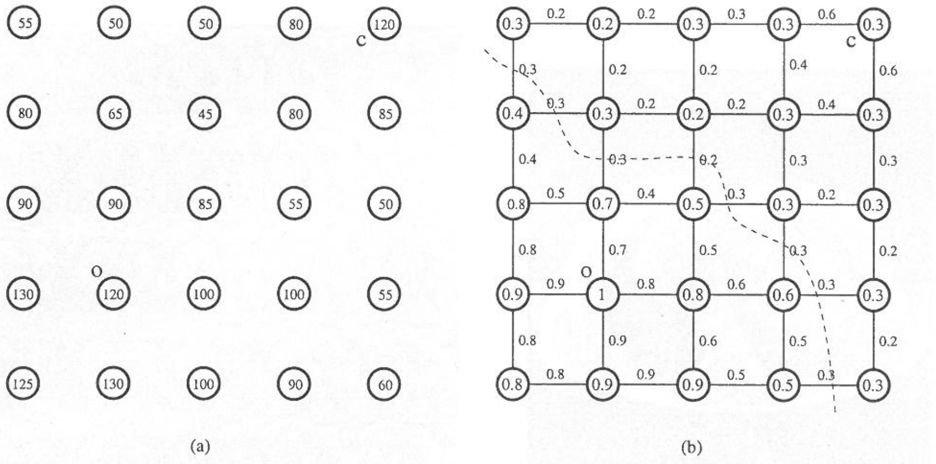

Fig. 3. Fuzzy object extraction. (a) grid point 'o' is a point over the object of interest (initial point for the algorithm). (b) in the resulted grid, a measure of connectedness is attributed to each grid point. Values over the connections between grid points are the affinity measures between them.

3(b)). Each such path is formed from a sequence of links between successive grid points in the path. Each link has the "strength" which is simply the affinity between the corresponding two grid points. The strength of a path is simply the strength of the weakest link in it. Finally, the strength of connectedness between o and c is the strength of the strongest of all paths. In defining a fuzzy object, the strength of connectedness between all possible pairs of grid points must be taken into account. Although this task involves problems of enormous combinatorial complexity, using dynamic programming [Cormen et al. 1991] reduces it dramatically, leading to reasonable computational times.

3.2. Results

A 4D form of the fuzzy object extraction algorithm has been used in our application (see Appendix A for an example of the algorithm). The algorithm is initialized by interactive selection of a pixel placed inside the cardiac muscle using marker in a slice (Fig. 4(a)). The same functions as Eq. 6 and Eq. 7 and 8-adjacency (in 4D) have been used to calculate the affinity between each pair of points. The mean value m is obtained by the intensity lev el of the initial point and an experimental value has been selected for the standard deviation. Fig. 4(a) shows five slices of a SE transversal image. In the third image, the initial point has been highlighted by the letter 'o' placed inside the interventricular septum. Fig. 4(b) shows the resulting fuzzy connectedness images (values between 0 and 1 have been mapped to grey levels between 0 and 255). Bright regions in these images represent the points connec ted to the initial point. Note that because of the similarity in grey level information between points representing cardiac muscle and those of surrounding tissues (e.g. thorax), a large strength of connectedness has been attributed to the points in these regions. Images in Fig. 4(c) have been obtained by suppressing the points in the original images (Fig. 4(a)) for which the fuzzy connectedness value has been less than 0.1.

4. Epicardial Contour Detection

As already mentioned, complementary information might be needed for a complete segmentation of the heart because of the intensity pattern similarity between the heart and surrounding tissues. Based on 4D image information, several methods have been proposed to include motion information in the segmentation process. Boudraa *et al.* [Boudraa et al. 1993] proposed a Fourier analysis method and applied it to cardiac scintigraphic image (time) series to provide a phase image used as supplementary information in a fuzzy clustering algorithm to isolate cardiac chambers. In a different approach, [Gorce er al. 1997] applied the optical flow method to estimate three-dimensional cardiac velocity fields in a CT data of a canine heart. This method, based on a variational approach, is very sensitive to image noise. As MRI cardiac images have a low S/N, we developed a

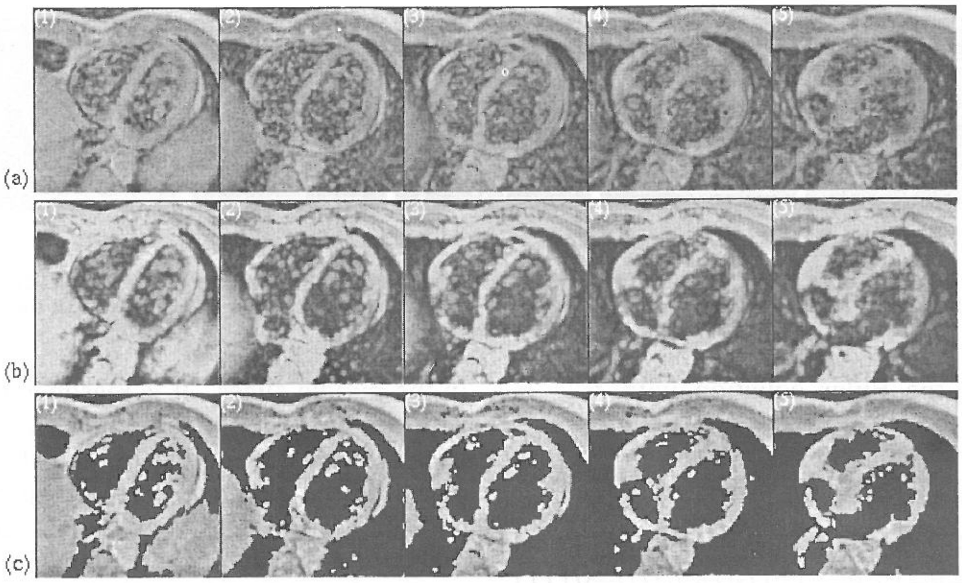

Fig. 4. Fuzzy object extraction algorithm. (a) Five slices of the original SE data. In the third image, 'o' shows the initial point selected inside the cardiac muscle, (b) the resulting connexity measures (values between 0 and 1 have been mapped to grey levels between 0 and 255), (c) the image obtained by suppressing the points in the original image for which fuzzy connectedness value has been less than 0.1. Noisy points inside the cardiac cavities have been eliminated.

method for epicardial boundary detection using motion information in the form of a variance image, assuming better efficiency in the presence of noise [Vaerman 1997]. The idea is to consider a stronger grey level variation for voxels representing the moving parts (cardiac muscle) compared to those representing stationary parts (e.g. thorax). We have obtained a variance image in which each voxel represents the variance of the same voxel in several images through different time phases. Bright regions at the center of the variance image in Fig. 5 represent the moving parts in the original image. We have applied an active contour model to obtain the contours of these bright regions which can represent a good estimation of the epicardial boundaries. In this section, we present a brief review of deformable contour model which will be followed by some details about contour propagation technique with demonstrating results.

4.1. Active Contour Model

A deformable contour is a planar curve which has an initial position and objective function associated with it. A special class of deformable contours called snakes was introduced by Kass *et al.* [Kass *et al.* 1987] in which the initial position is specified interactively by the user and the objective function is referred to as the energy of the snakes. Let $\upsilon(s) = (x(s), y(s))$ be the parametric description of the snake ($s \in [0, 1]$).

$$E_{snake} = \int_0^1 [E_{int}(\upsilon(s)) + E_{ext}(\upsilon(s))]ds \quad (8)$$

with:

$$E_{int}(s)=(\alpha(s)|\,\upsilon_s(s)\,|^2+\beta(s)|\,\upsilon_{ss}(s)\,|^2)/2 \quad (9)$$

$E_{int}(s)$ represents the internal energy of the active contour, $E_{ext}(s)$ represents external (image) forces, derivations are with respect to s, and $\upsilon(s)$ denotes a point along with the contour. The parameters $\alpha(s)$ and $\beta(s)$ influence the degree of smoothing. A large $\alpha(s)$ penalizes the development of positional discontinuities and encourages the contour's tendency to shrink. Similarly, a large $\beta(s)$ discourages sharp bends in the contour, whereas $\beta(s) = 0$ allows corners to develop. The external energy term in Eq. 8 is responsible for attracting the snake to the feature of interest in the image. The goal is to find the snake that minimizes Eq. 8 which is solved by using the calculus of variations and solving the following Euler-Lagrange equation for υ:

$$-(\alpha_{(s)}\upsilon')' + (\beta_{(s)}\upsilon'')'' + \nabla E_{ext}(\upsilon) = 0 \quad (10)$$

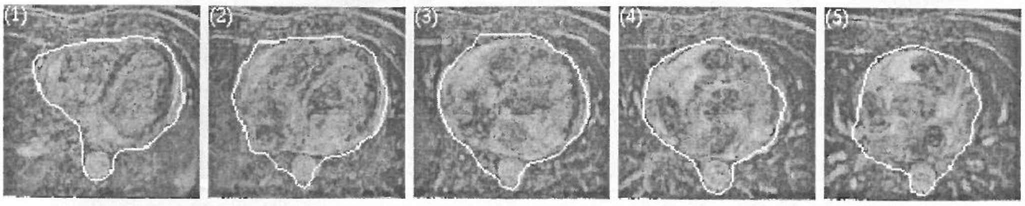

Fig. 5. Five different slices of the variance image. Each pixel represents the variance of the grey level of the same pixel in eight different images representing eight time phases of a cardiac cycle. Final positions of the snake have been superposed on each image.

Discretizing the Euler equation with $f_{x(i)} = \partial E_{ext}/\partial x_i$ and $f_{y(i)} = \partial E_{ext}/\partial y_i$,

$$\begin{aligned}&\alpha_i(v_i - v_{i-1}) - \alpha_{i+1}(v_{i+1} - v_i)\\&+\beta_{i-1}(v_{i-2} - 2v_{i-1} + v_i) - 2\beta_i(v_{i-1} - 2v_i + v_{i+1})\\&+\beta_{i+1}(v_i - 2v_{i+1} + v_{i+2}) + (f_x(i), f_y(i)) = 0 \quad (11)\end{aligned}$$

with $v(0) = v(n)$. Writing the equation in the matrix forms, one for x and another for y yields,

$$\mathbf{Ax} + \mathbf{f_x}(\mathbf{x}, \mathbf{y}) = 0 \quad (12)$$

$$\mathbf{Ay} + \mathbf{f_y}(\mathbf{x}, \mathbf{y}) = 0 \quad (13)$$

The final step is to solve for position vectors iteratively,

$$\mathbf{x}_t = (\mathbf{A} + \gamma\mathbf{I})^{-1}(\gamma\mathbf{x}_{t-1} - \mathbf{f_x}(\mathbf{x}_{t-1}, \mathbf{y}_{t-1})) \quad (14)$$

$$\mathbf{y}_t = (\mathbf{A} + \gamma\mathbf{I})^{-1}(\gamma\mathbf{y}_{t-1} - \mathbf{f_y}(\mathbf{x}_{t-1}, \mathbf{y}_{t-1})) \quad (15)$$

In our application, the image gradient has been used as external energy of snakes:

$$E_{ext} = E_{edge} = -|\nabla I(x, y)|^2 \quad (16)$$

The iterations converge to a local minimum of the energy field which must be in the vicinity of the border to be extracted. Checking for the convergence can be based on the total energy of the snake, with iterations being terminated when the change in energy is below the threshold. But in some cases the external forces can be large enough to make the snake oscillate around the equilibrium point. A more complete discussion and examples of algorithms for active contour models can be found in [Leroy et al. 1996].

4.2. Contour Propagation Technique

Propagation of epicardial boundaries along spatial direction through different slices [Ranganath 1995] is a part of the algorithm. In general, cardiac contours are more easily distinguishable in the middle slices. It is reasonable to propagate contours from the middle slice to the other slices. Extracted contour in each slice is superposed on the next one (spatial adjacent slices) and the algorithm is reexecuted. In order to maintain good stability for the system, for the results shown in this work, large coefficients have been used for internal energy components of the snake $(\alpha,\beta)=(10,10)$. The maximum number of iterations in each slice is set to 100 for the active contour algorithm. Fig. 5 shows five different slices of variance image with superposed detected contours. As external forces for the snake, we have used a binary image produced by simple thresholding of the variance image. A recursive implemented optimal gradient filter [Abrishami et al. 1994] has been used to produce gradient fields. Because of low spatial and temporal resolutions and low contrast and artifacts specially in GE images, the variance image is very noisy and specialist's interaction might be necessary for epicardial contour detection. Extracted contour in each slice is visualized and if necessary, the procedure can be recalled with a new initialization and different parameters. Fig. 6 presents an overview of the global segmentation algorithm.

5. Results and Discussion

In our experiments, two 4D cardiac data sets are used, a SE transversal image and a turboFLASH image in short axis view, both of healthy volunteers. The SE data has a domain of 256×256×8×8 with a voxel size of 1.25mm×1.25mm×10mm. The turboFLASH data has a domain of 256×256×9×10, obtained with TR/TE/Flip angle of 9ms/6ms/30° and a voxel size of 1.37mm×1.37mm×10mm. In both data sets the heart can be selected entirely by a matrix size of 110×110 pixels.

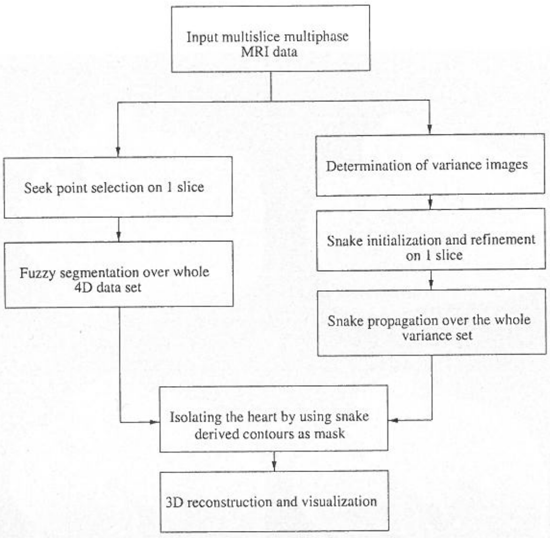

Fig. 6. An overview of the global segmentation algorithm.

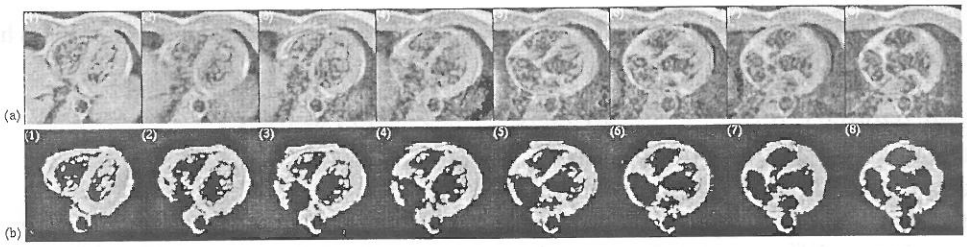

Fig. 7. (a) A number of slices from original SE data. Some of the slices have been obtained by interpolating the original data. (b) the result of fuzzy object extraction and active contour algorithms.

Before applying the fuzzy object extraction algorithm, the original grey level data is interpolated using second order interpolation technique to obtain cubic voxels. Using shape based interpolation of grey level images [Grevera and Udupa 1996] may improve the results presented in this work. The binary volumetric image obtained by active contour method has been interpolated using shape based interpolation [Raya and Udupa 1990]. We implemented fuzzy object extraction algorithms in 2, 3 and 4 dimensions within an internal version of the 3DVIEWNIX software system (Udupa *et al.* 1993) from which the 2D presentions have been obtained.

5.1. 2D Results

Performance of the algorithm was evaluated qualitatively using a series of 2D results. A clinical expert viewed the segmented images in both studies and indicated the images which appeared to be correctly segmented. The qualitative evaluation led to 90% and 85% visually acceptable segmented images for SE and turboFLASH studies, respectively. Many of the discrepancies between the expert's interpretation and the algorithm's results are related to apical and basal slices. At the apex level, the cavity does not appear in all of the volumes due to heart contraction. In general, epicardial contours are detected interactively at this level. Moreover, due to the echoes originated by papillary muscles, the cavity is not easily distinguishable from noisy points in this region. In basal slices, the presence of vessels, makes the procedure of epicardial boundary detection more complicated and in manually tracing, the expert tries to estimate the contour position by reviewing the preceding and subsequent images.

Fig. 7 compares the result of the algorithm with the original SE data. A number of intermediate slices which have been obtained by interpolation have been shown. In Fig. 7(b), bright regions inside the cavities may represent the papillary muscles or noisy points which have not been eliminated by the algorithm. In the absence of reliable low level constraints to distin-

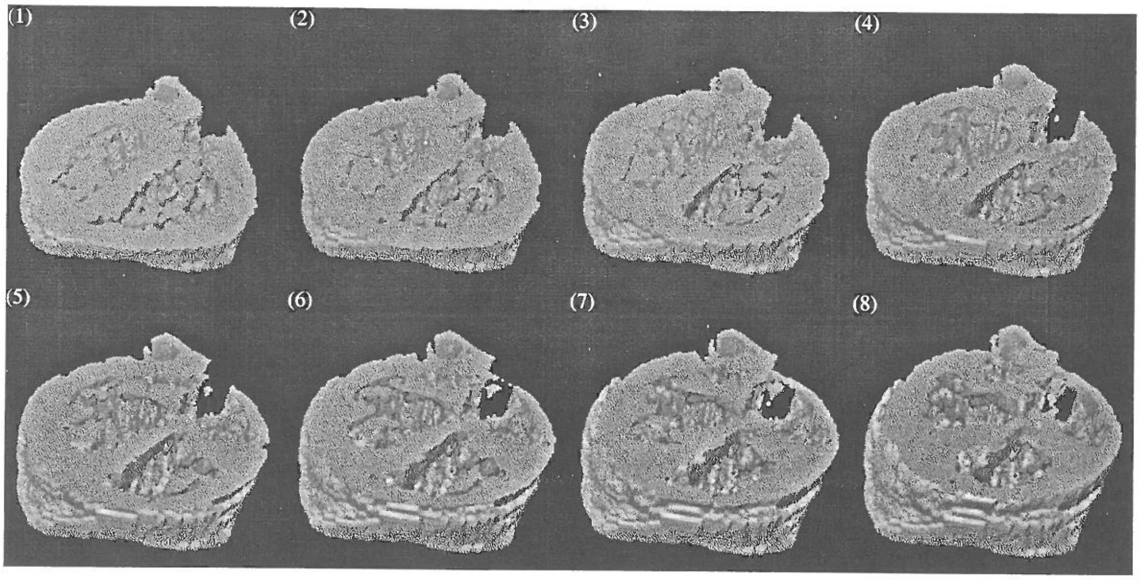

Fig. 8. Volume visualization of the heart using the SE data. For each image a different number of slices has been used.

guish between papillary muscles and artifacts, the algorithm make no explicit attempt to deal with papillary muscles. The specialist has the possibility to interactively suppress or preserve these points using a different minimum value for connectedness; however, large values may eliminate useful information of cardiac muscle. Bright regions attached to the epicardium represent fat tissues. The descending aorta is visible in all of the images.

5.2. 3D Results

Fig. 8 shows a volume visualization of the heart using the SE data. Each image has been obtained using a different number of slices. At the apex level, note the presence of papillary muscles inside the ventricular cavities. The descending aorta is visible at the top of all images. Fig. 9 presents a 3D visualization of the heart using the turboFLASH data. Two ventricles

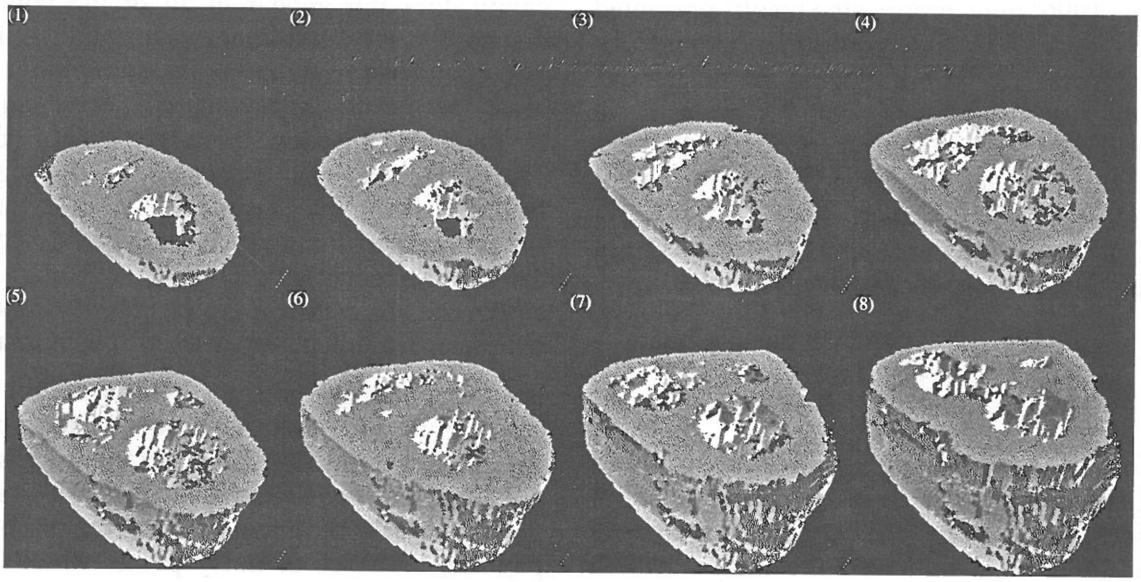

Fig. 9. Volume visualization of the heart using the turboFLASH data. For each image a different number of slices has been used.

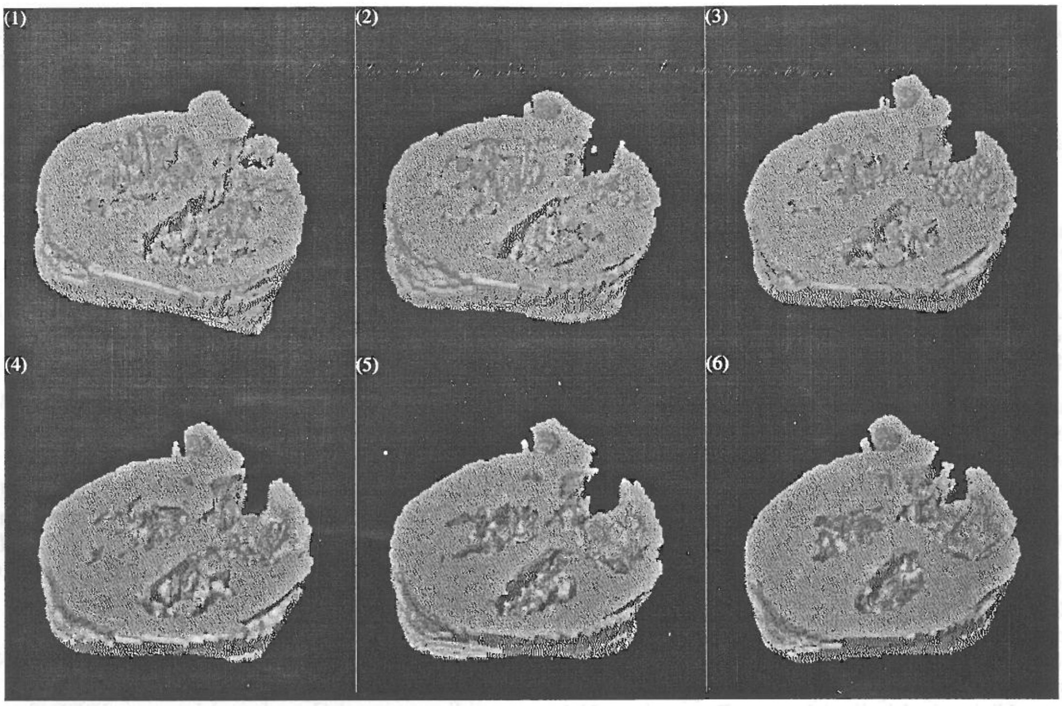

Fig. 10. Dynamic volume visualization of the heart using the axial SE data. Anatomical details of the heart through 6 different time phases from diastole to systole are visible.

are visible in these images. Because of the poor quality of the original data and blood movement artifacts, the right ventricle is not entirely visible in some of the images.

5.3. Dynamic Volume Visualization

Fig. 10 shows a volume visualization of the moving heart at 6 different time phases from diastole to systole, using the 4D SE data. Anatomical details of the heart, including ventricular muscles and interventricular septum in motion, are visible. The data in 3D presentations has been rendered by ray-tracing technique using the VOLVIS software system (Avila *et al.* 1994).

6. Concluding Remarks

Based on 4D data available by cardiac MRI, we developed a system for dynamic anatomical volume visualization of the heart in which minimum interaction of a specialist is necessary. Segmented 2D images obtained by the algorithm are well correlated with original 2D slices reviewed by a specialist. Our data set was very limited to do a complete analysis and, moreover, a study of variation in the results obtained by different observers is necessary to gain a better idea about the error resulted by the algorithm. The algorithm is relatively fast. On a classic workstation the run time for a 4D version of the fuzzy object extraction algorithm is about 3 minutes for a threshold value of 0.1.

Characterizing ventricular wall motion is of great importance for the diagnosis of local abnormalities in the myocardium thickening. This will be the next part of our work which necessitates automatic extraction of quantitative information of the LV motion using fuzzy approach, which is a complex task, especially in gradient echo images.

Acknowledgements This work is in the scope of the scientific topics of the PRC-GDR ISIS research group of the French National Center for Scientific Research (CNRS). It was supported in part by the regional council of Picardie. The authors gratefully acknowledge Dr. Y. Maingourd for his contribution to this work and Professor I. Idy-Peretti for her help in data acquisition. We would like to thank CREATIS CNRS research unit, France, and MIPG of the University of Pennsylvania for supplying images, and also Ms. Malgouyres from Siemens France for

supplying helpful information on data acquisition.

References

[Abrishami et al. 1996] H. ABRISHAMI AND J. F. LERALLUT AND Y. MAINGOURD (1996), Detection and Time-Tracking of Cardiac Boundaries in MRI 4D Data Using Snakes, In Proceedings, 18th Annual International Conference of IEEE EMBS, Amsterdam, pp. 728–729.

[Abrishami et al. 1994] H. ABRISHAMI AND J. F. LERALLUT AND L. ROBERT AND Y. MAINGOURD (1994), An efficient algorithm for endocardial boundary detection in two-dimensional echocardiography, In Proceedings, 16th Annual International Conference of IEEE EMBS, Baltimore, pp. 712–713.

[Amini et al. 1994] A. A. AMINI AND R. W. CURWEN AND R. T. CONSTABLE AND J. C. GORE (1994), MR Physics-Based Snake Tracking and Dense Deformations from Tagged Cardiac Images, In Technical Report of AAAI Spring Symposium: Applications of Computer Vision in Medical Image Processing, Vol. SS–94–05, The AAAI Press, pp. 126–130.

[Avila et al. 1994] R. AVILA AND T. HE AND L. HONG AND A. KAUFMAN AND H. PFISTER AND C. SILVA AND L. SOBIERAJSKI AND S. WANG (1994), VolVis: A Diversified Volume Visualization System, R. Bergeron and A. Kaufman (Eds.), In Proceedings Visualization '94, IEEE Computer Society Press, pp. 31–38,

[Axel and Dougherty 1989] L. AXEL AND L. DOUGHERTY (1989), MR imaging of motion with spatial modulation of magnetization, *Radiology*, **171**, 841–845.

[Bardinet et al. 1994] E. BARDINET AND N. AYACHE AND L. D. COHEN (1994), Fitting of iso-surfaces using superquadrics and free-form deformations, In Proceedings of IEEE Workshop on Biomedical Image Analysis, Seattle, WA, pp. 184–193

[Boudraa et al. 1993] A. O. BOUDRAA AND J. J. MALLET AND J. E. BESSON AND S. BOUYOUCEF AND J. CHAMPIER (1993), Left ventricle automated detection method in gated isotopic ventriculography using fuzzy clustering, *IEEE Transactions on Medical Imaging*, **12**(3), 451–465.

[Chakraborty et al. 1996] A. CHAKRABORTY AND L. H. STAIB AND J. S. DUNCAN (1996), Deformable Boundary Finding in Medical Images by Integrating Gradient and Region Information, *IEEE Transactions on Medical Imaging*, **15**(6), 768–785.

[Cohen et al. 1992] I. COHEN AND L. D. COHEN AND N. AYACHE (1992), Using Deformable Surfaces to Segment 3D Images and Infer Differential Structures, *Computer Vision, Graphics and Image Processing: Image Understanding*, **56**(2), 242–263.

[Cohen and Cohen 1990] L. D. COHEN AND I. COHEN (1990), A finite element method applied to new active contour models and 3–D reconstruction from cross sections, In Proceedings, Third International Conference on Computer Vision, Computer Society Conference, Osaka, Japan, pp. 587–591.

[Cormen et al. 1991] T. CORMEN AND C. LEISERSON AND R. RIVEST (1991), *Introduction to Algorithms*, McGraw–Hill, New York.

[Declerck et al. 1996] J. DECLERCK AND J. FELDMAR AND N. AYACHE (1996), Definition of a 4D continuous polar transformation for the tracking and the analysis of LV motion, Tehnical Report 3039, INRIA.

[Desgrez et al. 1994] A. DESGREZ AND J. BITTOUN AND I. IDY–PERETTI (1994), *Cahiers d'IRM: 1. Bases Physiques de l'IRM*, 2nd edn., Masson, Paris.

[Edelman 1995] R. R. EDELMAN (1995), *Fast Magnetic Resonance Imaging: A Primer*, SIEMENS.

[Gorce er al. 1997] J. M. GORCE AND D. FRIBOULET AND I. E. MAGNIN (1997), Estimation of three-dimensional cardiac velocity fields: assessment of a differential method and application to three-dimensional CT data, *Medical Image Analysis*, **1**(3), 245–261.

[Grevera and Udupa 1996] G. J. GREVERA AND J. K. UDUPA (1996), Shape-Based Interpolation of Multidimensional Grey-Level Images, *IEEE Transactions on Medical Imaging*, **15**(6), 881–892.

[Höhne 1995] K. H. HÖHNE (1995), *VOXEL-MAN, Part 1: Brain and Skull, Version 1.0*, Springer–Verlag Electronic Media, Heidelberg.

[Höhne et al. 1992] K. H. HÖHNE AND A. POMMERT AND M. RIEMER AND TH. SCHIEMANN AND R. SCHUBERT AND U. TIEDE AND W. LIERSE (1992), Framework for the generation of 3D anatomical atlases, In Proceedings: Visualization in Biomedical Computing, Vol. SPIE 1808, Chapel Hill, NC, pp. 510–520.

[Irarrazabal et al. 1995] P. IRARRAZABAL AND T. SACHS AND C. MEYER AND J. BRITTAIN AND D. NISHIMURA (1995), Fast Volumetric Imaging of the Heart, In Proceedings, Third Annual Meeting of the Society of Magnetic Resonance in Medicine, Nice, France.

[Kass et al. 1987] M. KASS AND A. WITKIN AND D. TERZOPOULOS (1987), Snakes: Active contour models, *International Journal of Computer Vision*, **1**, 321–331.

[Kaufmann 1975] A. KAUFMANN (1975), *Introduction to the Theory of Fuzzy Subsets*, Academic Press, Vol I, New York.

[Leroy et al. 1996] B. LEROY AND I. L. HERLIN AND L. D. COHEN (1996), Multi-resolution algorithms for active contour models, In Proceedings of 12th International Conference on Analysis and Optimization of Systems: Images, Wavelets and PDE's (ICAOS'96), Paris.

[McInerney and Terzopoulos 1993] T. MCINERNEY AND D. TERZOPOULOS (1993), A finite element model for 3–D shape reconstruction and non-rigid motion tracking, In Proceedings of 4th International Conference on Computer Vision, Berlin, Germany, pp. 518–523.

[McVeigh et al. 1994] E. McVeigh and M. Guttman and E. Poon and P. Chandrasekhar and C. Moore and E. Zerhouni and M. Solayappan and P. A. Heng (1994), Visualization and analysis of functional cardiac MRI data, In SPIE Proceedings, Vol 2168.

[Park et al. 1996a] J. Park and D. Metaxas and A. A. Young and L. Axel (1996a), Deformable Models with Parameter Functions for Cardiac Motion Analysis from Tagged MRI Data, *IEEE Transactions on Medical Imaging*, **15**(3), 278–289.

[Park et al. 1996b] J. Park and D. Metaxas and L. Axel (1996b), Analysis of left ventricular wall motion based on volumetric deformable models and MRI-SPAMM, *Medical Image Analysis*, **1**(1), 53–71.

[Pauly et al. 1996] J. Pauly and C. Hardy and C. Meyer and D. Nishimura and A. Macovski (1996), Real-Time Dynamic Imaging on a Conventional Whole-Body Imaging System, In Proceedings, 4th Annual Meeting of International Society for Magnetic Resonance in Medicine, New York.

[Ranganath 1995] S. Ranganath (1995), Contour Extraction from Cardiac MRI Studies Using Snakes, *IEEE Transactions on Medical Imaging*, **14**(2), 328–338.

[Raya and Udupa 1990] S. P. Raya and J. K. Udupa (1990), Shape-Based Interpolation of Multidimensional Objects, *IEEE Transactions on Medical Imaging*, **9**(1), 32–42.

[Shi et al. 1994] P. Shi and G. Robinson and J. Duncan (1994), Mayocardial Motion and Function Assessment Using 4D Images, In Proceedings: Visualization in Biomedical Computing, Vol. SPIE 2359, Dallas, TX, pp. 148–159.

[Siemens 1992] (1992) *Advanced MR Cardio Guide for the MAGNETOM*, SIEMENS.

[Terzopoulos et al. 1988] D. Terzopoulos and A. Witkin and M. Kass (1988), Constraints on deformable models: Recovering 3–D shape and nonrigid motion, *AI Journal*, **36**, 91–123.

[Terzopoulos and Metaxas 1991] D. Terzopoulos and D. Metaxas (1991), Dynamic 3D Models with Local and Global Deformations: Deformable Superquadrics, *IEEE Transactions on Pattern Analysis and Machine Intelligence*, **13**(7), 703–714.

[Udupa and Samarasekera 1996] J. K. Udupa and S. Samarasekera (1996), Fuzzy Connectedness and Object Definition: Theory, Algorithms, and Applications in Image Segmentation, *GRAPHICAL MODELS AND IMAGE PROCESSING*, **58**(3), 246–261.

[Udupa et al. 1993] J. K. Udupa and R. J. Goncalves and K. Iyer and S. Narendula and D. Odhner and S. Samarasekera ans S. Sharma (1993), 3DVIEWNIX: An Open, transposable software system for the visualization and analysis of multidimensional, multimodality, multiparametric images, In SPIE Proceedings, Vol. 1897, pp. 47–58.

[Vaerman 1997] V. Vaerman (1997), Unsupervised segmentation of the human heart using deformable contours, In Proc. of the World Congress on Medical Physics and Biomedical Engineering, Vol. 2, Nice, France, p. 634.

[Vannier et al. 1989] M. Vannier and C. Hildebolt and J. Marsh and T. Pilgram and W. McAllister and G. Shackelford and C. Offutt and R. Knapp (1989), Craniosynostosis: Diagnostic value of three-dimensional CT reconstruction, *Radiology*, **173**, 669–673.

[Zadeh 1965] L. A. Zadeh (1965), Fuzzy Sets, *INFORMATION AND CONTROL*, **8**, 338–353.

[Zerhouni 1988] E. A. Zerhouni and D. M. Parish and W. J. Rogers and A. Yang (1988), Human heart: Tagging with MR imaging-A method for noninvasive assessment of myocardial motion, *Radiology*, **169**, 59–63.

APPENDIX A

A *fuzzy connected object* $\mathcal{O}$ of a scene domaine $\mathcal{C}$ of strength $\theta_x = [x, 1]$, $0 \leq x \leq 1$, and containing a pixel o consists of a pool $O \subset C$ of pixels together with a value indicating "objectness" assigned to every pixel. O is such that $o \in O$, for any pixel c and d in O, the strength of connectedness between them $\mu_\kappa(c, d) \geq x$, and for any pixels $c \in O$ and $e \notin O$, the strength $\mu_\kappa(c, e) < x$. The value of obje ctness assigned to pixels in O varies between 0 and 1 and the value assigned to pixels outside O is 0.

For completeness, we reproduce below one of the algorithms described in [Udupa and Samarasekera 1996], which, given $\mathcal{C}$, κ, θ_x, and o extracts a fuzzy object containing o. Note that, before entering step 8 in the algorithm, the fuzzy object information is available in the form of a "connectivity scene" $\mathcal{C}_o = (C_o, f_o)$, where $C_o = C$ and for any $c \in C_o$, $f_o(c) = \mu_\kappa(o, c)$. That is, in this scene, intensity is proportional to "hanging-togetherness" (Fig. 4(b)).

Algorithm: Fuzzy Object Extraction, $\kappa\theta_x FOE$.
Input: $\mathcal{C}$, o, κ and θ_x as defined above.
Output: Fuzzy object of $\mathcal{C}$ of strength θ_x containing o.
Auxiliary Data Structures: An nD array representing the connectivity scene $\mathcal{C}_o = (C_o, f_o)$ of $\mathcal{C}$ and a queue Q of pixels. We refer to the array itself by $\mathcal{C}_o$ for the purpose of the algorithm.

```
begin
    0. set all elements of $C_o$ to 0 except $o$ which is set to 1;
    1. push all pixels $c \in C_o$ such that $\mu_\kappa(o, c) > 0$ to $Q$;
      while $Q$ is not empty do
    2.     remove a pixel $c$ from $Q$;
    3.     if $f_o(c) < x$ then
    4.         find $f_{max} = \max_{d \in C_o}[min(f_o(d), \mu_\kappa(c, d))]$;
    5.         if $f_{max} > f_o(c)$ and $f_{max} \geq x$ then
    6.             set $f_o(c) = f_{max}$;
    7.             push all pixels $e$ such that $\mu_\kappa(c, e) > 0$ to Q;
               endif;
           endif;
      endwhile;
    8. Output the fuzzy object containing $o$ from the information in $C_o$;
end.
```

Received: May, 1997
Revised: February, 1998
Accepted: April, 1998

Contact address:

Jean–Francois Lerallut
Universite de Technologie de Compiegne
Departement de Genie Biologique
UMR CNRS 6600
BP 20529
60205 Compiègne Cedex
France
phone: +33 (0)3 44 23 43 91
fax: +33 (0)3 44 20 48 13
e-mail: lerallut@utc.fr

HAMID ABRISHAMI MOGHADDAM was born in Iran in 1964. He received his B.B. and M.S. degrees in Electrical Engineering from Amirkabir (1988) and Sharif (1991) Universities, Teheran, Iran. Curently, he is working on multidimensional medical image processing at the Université de Technologie de Compiègne where he obtained his Ph.D. degree in Biomedical Engineering (1998).

JEAN–FRANCOIS LERALLUT was born in France in January 1953. He received an Engineering degeree in Electronics from ESME in 1976, and a Doctorate in Engineering in 1979. Presently he is Professor in Biomedical Engineering Department at the Université de Technologie de Compiègne and manages a research group on medical image processing.